Magnetoactive asymmetric mechanical metamaterial for tunable elastic cloaking

Quan Zhang [a, *], Gengkai Hu [b], Stephan Rudykh [a, c]

[a] *School of Mathematical and Statistical Sciences, University of Galway, Galway, H91 TK33, Ireland*

[b] *School of Aerospace Engineering, Beijing Institute of Technology, Beijing, 100081, China*

[c] *Department of Mechanical Engineering, University of Wisconsin – Madison, Madison, WI 53706, United States*

ABSTRACT

We propose a magnetic field-induced asymmetric mechanical metamaterial for tunable transformation-based elastic cloaking. The metamaterial is designed by integrating hard-Magnetic Active Elastomers (hMAEs) and combining zero-stress collapse modes to produce a unique asymmetric behavior controlled by an external magnetic field. The relationship bridging the microstructure and the desired cloaking performance is presented. This magneto-metamaterial design is applied to achieve tunable static elastic cloaking. The theoretical predictions, together with the numerical tests under various static loads, demonstrate encouraging cloaking performance. The study also highlights the impact of magneto-mechanical coupling and offers the first remotely-controllable hMAE-based cloaking solution, with promising potential in various applications including stress shielding and stealth technologies.

Keywords: hard-magnetic; mechanical metamaterials; magnetoactive elastomers; transformation method; elastic cloaks

1 Introduction

Mechanical metamaterials can produce a variety of desirable properties and functions through their engineered underlying microstructure (Bertoldi et al., 2017; Krushynska et al., 2023): from subwavelength waveguiding (Bilal et al., 2017b; Wang et al., 2016; Zhu et al., 2014) and focusing (Memoli et al., 2017), topologically protected transportation (Chen et al., 2019; Chen et al., 2021b;

* Corresponding author:
E-mail address: quan.zhang@universityofgalway.ie, zhangquanbit@gmail.com (Q. Zhang)

Wang et al., 2015; Zhang et al., 2020b; Zhang et al., 2018), energy absorption (Pan et al., 2019; Wang et al., 2019), to vibration switching (Bilal et al., 2017a; Gross et al., 2023; Wei et al., 2021) and isolation (Liu et al., 2019; Zhang et al., 2021). Moreover, metamaterials brought to life the prospect of realization of the invisibility cloak beyond science fiction. A cloak is a special coating medium designed to make an object completely invisible to its surroundings. This is achieved by applying a geometric transformation that enlarges a point in the background and maps it onto the cloak inner boundary. Through this process, the properties of the cloak material in the physical domain can be revealed by the transformed governing equations. The so-called transformation method, originally introduced for conductivity (Greenleaf et al., 2003) and geometric optics (Leonhardt, 2006), has been successfully applied to other classic physical areas such as electromagnetism (Ergin et al., 2010; Pendry et al., 2006), acoustics (Chen et al., 2017; Cummer and Schurig, 2007; Norris, 2008), and elasticity (Brun et al., 2009; Buckmann et al., 2015; Buckmann et al., 2014; Milton et al., 2006).

For elastic cloaking in solids, the coating material is required to obey unusual constitutive behavior, which is contingent upon the gauge chosen to monitor the migration of displacement vector from the virtual space to the transformed space. The necessary transformation material for a perfect elastic cloak cannot be designed with the means of classical elasticity, thus, pushing the exploration beyond the limits of Cauchy materials. The alternatives include either (*i*) Willis' materials (Milton et al., 2006) (coupling stress with velocity and momentum with strain) or (*ii*) the asymmetric medium (Brun et al., 2009) (lacking minor symmetry of the elasticity tensor). The use of Willis' materials poses difficulties in mapping periodic structures onto an effective Willis medium description, since the required high-frequency homogenization is challenging in the limit with strong Willis's coupling effects. The asymmetric medium (characterized by the asymmetric elasticity tensor) is directly available within the framework of micropolar theory; however, recent studies indicate that the full Cosserat theory does not maintain form-invariance when subjected to a general space mapping, posing challenges in designing an elastic cloak using this theory (Zhang et al., 2020a). Besides, it is worth noting that the small-on-large theory offers a viable approach for designing elastic cloaks; as an example, the tangent moduli of pre-stressed semi-linear hyperelastic materials have the potential to meet the requirement defined by transformation theory – lacking minor symmetry (Guo et al., 2022; Norris and Parnell, 2012; Parnell, 2012). Such materials, maintaining a linear stress-strain, are difficult to achieve in the nonlinear regime of finite strains.

To comprehend how breaking the symmetry of stresses can lead to cloaking in solids, one must examine the fundamental principle governing stress symmetry, that is, the local balance of angular momentum. To achieve elastic cloaking, it is necessary to find microstructures that enable to maintain the balance of angular momentum in a unique manner. The core idea revolves around applying a carefully engineered distribution of body torques with sufficient strength to modify the balance of angular momentum (Nassar et al., 2020). Potentially, the necessary torques can be produced by leveraging grounded torsional springs (Nassar et al., 2018, 2019; Xu et al., 2020). These works make an important step towards elastic cloaking design. However, the required grounding infrastructure could introduce significant levels of complexity. An alternative approach can employ the rotational resonance effect (Nassar et al., 2020; Zhang et al., 2020a). Such elastic cloak operates at a single rotational resonant frequency only, and may not be applicable for the static case.

Here, we put forward a novel design of magnetoactive mechanical metamaterials with intriguing symmetry-breaking properties, building on the rich physics offered by the unusual behavior of *hard*-Magnetic Active Elastomers (hMAEs). Such active materials consist of a soft elastomer matrix embedded with hard-magnetic particles (Kim et al., 2018; Lum et al., 2016). The application of external magnetic fields generates micro torques on the embedded hard-magnetic particles. This microscopic effect results in macroscale responses of the hMAE composite, leading to complex shape transformations (Goshkoderia et al., 2020; Lucarini et al., 2022; Moreno-Mateos et al., 2022; Mukherjee et al., 2021; Yan et al., 2021a; Yan et al., 2023; Yan et al., 2021b; Zhao et al., 2019). The rapid, reversible, and remotely-controlled shape-transforming behavior of hMAEs has enabled functionalities in areas such as soft robotics (Hu et al., 2018), biomedical devices (Wang et al., 2021) and metamaterials (Chen et al., 2021a; Montgomery et al., 2020; Zhang et al., 2023a; Zhang et al., 2023b; Zhang and Rudykh, 2022). In particular, magneto-mechanical coupling has been shown to be a promising strategy for designing tunable and active metamaterials, owing to its distinct advantages for shape reconfiguration and property tuning (Alam et al., 2023; Kheybari and Bilal, 2023; Sim et al., 2023; Sim and Zhao, 2023; Wang et al., 2023; Wang et al., 2020; Watkins et al., 2022; Yang and Keten, 2023; Zhang et al., 2023c). There have been efforts to undertake pertinent experimental research (Lee et al., 2022; Sim et al., 2023; Watkins et al., 2022). In this study, we propose to exploit the field-controllable magnetic body torque to modify the very form of the elasticity tensor, enabling elastic cloaking. We illustrate how the spatial gradient of magnetoactive

asymmetric metamaterials can effectively control the distribution of displacement and stress in the vicinity of a cloaked region. The remote and reversible principle of activation eliminates the need for grounding infrastructure or rotational resonance, thus, providing the first remotely-controllable hMAE-based cloaking solution.

2 Asymmetric medium for elastic cloaking

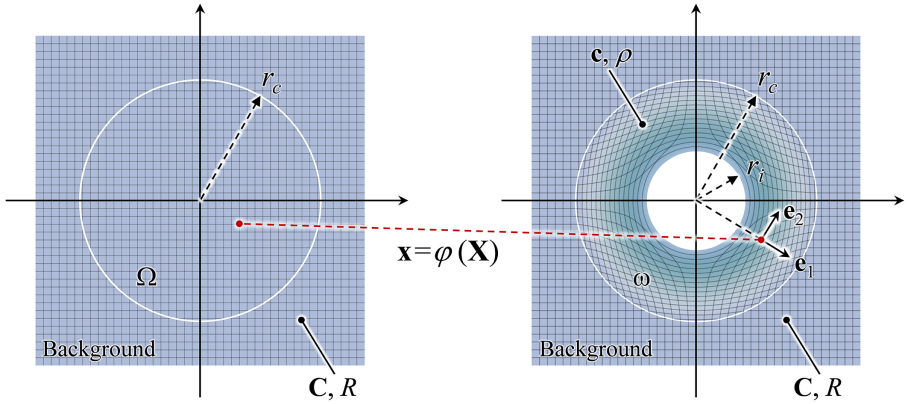

Fig. 1. Schematics of the transformation method. The geometric transformation φ maps a point **X** of the reference medium Ω into point **x** of the physical medium ω. The physical medium (i.e., the cloak) is characterized by an inner radius r_i and an outer radius r_c. The elastic tensor and density in the background and undeformed domain are denoted by **C** and R, respectively. In the transformed domain, they are represented by **c** and ρ, respectively.

The transformation method for an elastic cloaking is illustrated in Fig. 1. Consider a geometric transformation φ that maps from the reference medium Ω to the physical medium ω. The two media share the same shape and composition over the background region, but they exhibit difference within a cloak area. The cloak area is characterized by an inner radius r_i and an outer radius r_c. Here we employ the gauge that requires parallel displacement migration between the original and transformed domains (Brun et al., 2009), i.e., **u**(**x**) = **U**(**X**), the transformed elasticity tensor **c** corresponding to a classical elastic medium (with symmetric elasticity tensor **C**) is $c_{ijkl} = J^{-1}F_{ip}C_{pjql}F_{kq}$. $\mathbf{F} = \partial\mathbf{x}/\partial\mathbf{X}$ is the transformation gradient, and J = det **F** is the Jacobian of transformation. Note that the transformed elasticity tensor **c** no longer exhibits minor symmetry because the geometric transformation **F** does not equally act on the subscripts. In what follows, we consider the background to be homogenous and isotropic (with Lame's constants λ and μ), and cloaking transformation is axisymmetric. Therefore, the constitutive relation of the coating medium can be expressed in Voigt form as (Brun et al., 2009)

$$\begin{bmatrix}\sigma_{11}\\ \sigma_{22}\\ \sigma_{12}\\ \sigma_{21}\end{bmatrix}=\begin{bmatrix}(2\mu+\lambda)g & \lambda & 0 & 0\\ \lambda & (2\mu+\lambda)/g & 0 & 0\\ 0 & 0 & \mu g & \mu\\ 0 & 0 & \mu & \mu/g\end{bmatrix}\begin{bmatrix}e_{11}\\ e_{22}\\ e_{12}\\ e_{21}\end{bmatrix},\quad g=\frac{\|\mathbf{x}\|-r_i}{\|\mathbf{x}\|}, \tag{1}$$

where the displacement gradient component $e_{ij} = u_{j,i}$. To illustrate the stress asymmetric effect, consider the displacement gradient with components $e_{11} = e_{22} = 0$ and $e_{21} = -e_{12} = \phi$ (corresponding to an infinitesimal plane rotation), one obtains $\sigma_{12} - \sigma_{21} = (2c_{1221} - c_{1212} - c_{2121})\phi \neq 0$. This implies that when a rotation occurs, restoring body torque emerges in response. Moreover, since **c** is of rank 3, the cloaking materials must accommodate one zero mode (Nassar et al., 2018). One can obtain through Eq. (1) that the unique zero mode is $\mathbf{e}_{zm} = \mathbf{e}_1 \otimes \mathbf{e}_2 - g\mathbf{e}_2 \otimes \mathbf{e}_1$ ($\mathbf{e}_1$ and $\mathbf{e}_2$ are the polar basis as illustrated in Fig. 1), satisfying $\mathbf{ce}_{zm} = \mathbf{0}$.

3 Magnetoactive asymmetric mechanical metamaterials

3.1 The lattice model and analytical homogenization

To realize the required transformation medium, we propose a novel design of magnetoactive asymmetric mechanical metamaterial (MAMM). As shown in Fig. 2a, the performance of the MAMM-based elastic cloak can be tuned by external magnetic fields. The magneto-mechanical response of the MAMM is described by the mass-spring model depicted in Fig. 2b. Note that we consider a lattice similar to the one studied by (Nassar et al., 2018), where they achieved the asymmetric effect in their purely mechanical study by introducing external grounded springs. Here we put forward the new concept of using the magnetic body torque to eliminate the need for grounding infrastructure. Each unit cell comprises two diagonal springs with a constant α, one vertical spring with a constant β, and a mass block made of hMAE. The hMAE blocks are characterized by the remanent magnetization **M**, and its direction in the undeformed state is aligned with the direction of the external magnetic field **B**. Once the lattice is deformed under mechanical loadings, the rotating hMAE block will be exerted with a restoring magnetic body torque $MB\phi$, with ϕ being the infinitesimal rotation angle, as illustrated in Fig. 2c. Therefore, the magneto-mechanical coupling effect can be equivalently considered as that the mass block is connected with a *virtual* grounded torsional spring with the stiffness of MB. Besides, all connections (springs α, β) are assumed to be hinge-like, enabling the required zero mode (Nassar et al., 2018).

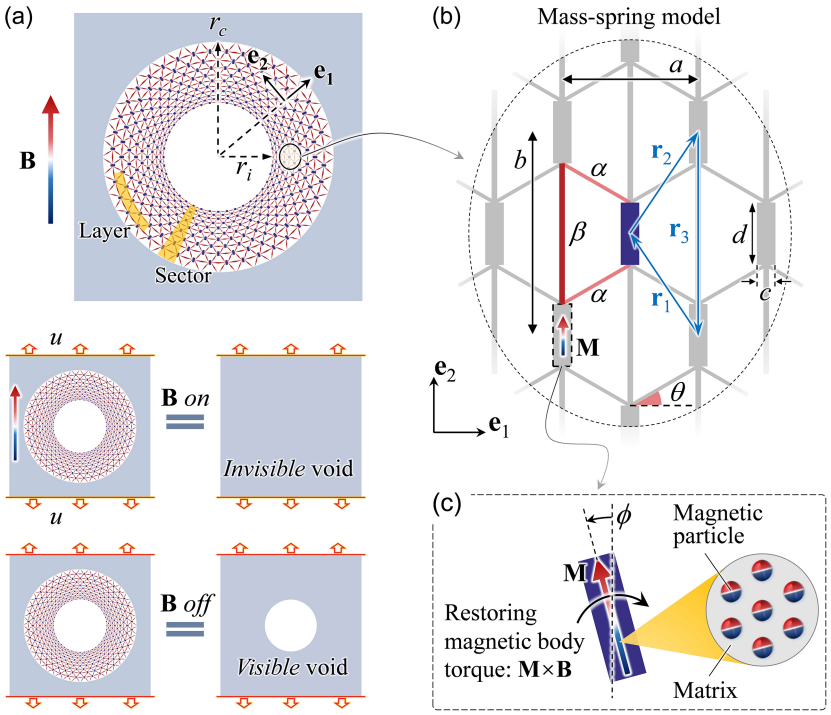

Fig. 2. The proposed magnetoactive asymmetric mechanical metamaterial and its application to elastic cloaking. (a) The cloak system is illustrated with a void enveloped by the proposed magnetoactive asymmetric metamaterial, all within an isotropic background. The performance of the elastic cloak can be tuned by external magnetic fields. (b) The representative mass-spring model consists of springs represented by the straight edges and mass blocks made of hMAEs represented by the rectangles; note that all connections between components are hinge-like. (c) The hMAE blocks are characterized by the remanent magnetization **M**, and its direction in the reference (undeformed) configuration is aligned with the direction of the external magnetic field **B**. Once the lattice is deformed under mechanical loading, the rotating hMAE block will be exerted with a restoring magnetic body torque $MB\phi$, with ϕ being the infinitesimal rotation angle.

Following the purely mechanical work by (Nassar et al., 2018), we examine the effective elasticity tensor of the proposed magnetoactive lattice system. Consider that the MAMM is subjected to a uniform displacement gradient $\mathbf{e}=(\nabla\mathbf{u})^T$ and all mass blocks experience a rotation of angle ϕ during deformation, the *total* potential energy per unit area can be written as $\psi=\psi_\alpha+\psi_\beta+\psi_M$. The first term represents the mechanical energy stored in the springs with constant α, the second term represents the mechanical energy stored in the spring with constant β, and the last term represents the magnetic potential energy. One can obtain that

$$\begin{aligned}
\psi_\alpha &= \frac{\alpha}{2V}\left[\left(\mathbf{e}^T\mathbf{r}_1+d\phi\mathbf{e}_1\right)\cdot\mathbf{e}'_\theta\right]^2+\frac{\alpha}{2V}\left[\left(\mathbf{e}^T\mathbf{r}_2+d\phi\mathbf{e}_1\right)\cdot\mathbf{e}_\theta\right]^2,\\
\psi_\beta &= \frac{\beta}{2V}\left[\mathbf{e}^T\mathbf{r}_3\cdot\mathbf{e}_2\right]^2,\\
\psi_M &= \frac{MB\cdot cd}{2V}\phi^2,
\end{aligned}\tag{2}$$

where $V = ab/2$ is the effective area of the unit cell; c and d are the side lengths of the hMAE mass block, and $d = \left(b\cos\theta - a\sin\theta\right)/\left(2\cos\theta\right)$; $\mathbf{r}_1 = -a\mathbf{e}_1/2+b\mathbf{e}_2/2$, $\mathbf{r}_2 = a\mathbf{e}_1/2+b\mathbf{e}_2/2$, and $\mathbf{r}_3 = -b\mathbf{e}_2$ are the lattice vectors; $\mathbf{e}_\theta = \cos\theta\mathbf{e}_1 + \sin\theta\mathbf{e}_2$ and $\mathbf{e}'_\theta = -\cos\theta\mathbf{e}_1 + \sin\theta\mathbf{e}_2$. Note that at equilibrium, we have $\partial\psi/\partial\phi = 0$. This implies

$$\phi = -\frac{\cos\theta\left(a\sin\theta e_{12} + b\cos\theta e_{21}\right)\alpha}{\cos\theta\left(b\cos\theta - a\sin\theta\right)\alpha + MBc}. \tag{3}$$

The Hooke's law $\boldsymbol{\sigma} = \partial\psi/\partial\mathbf{e}$ for the MAMM lattice is then written as

$$\begin{bmatrix}\sigma_{11}\\ \sigma_{22}\\ \sigma_{12}\\ \sigma_{21}\end{bmatrix} = \begin{bmatrix} \frac{a\alpha\cos^2\theta}{b} & \alpha\cos\theta\sin\theta & 0 & 0 \\ \alpha\cos\theta\sin\theta & \frac{b\left(\alpha\sin^2\theta+2\beta\right)}{a} & 0 & 0 \\ 0 & 0 & \frac{ac\alpha MB\sin^2\theta}{2bd\alpha\cos^2\theta+MBbc} & \frac{c\alpha MB\cos\theta\sin\theta}{2d\alpha\cos^2\theta+MBc} \\ 0 & 0 & \frac{c\alpha MB\cos\theta\sin\theta}{2d\alpha\cos^2\theta+MBc} & \frac{bc\alpha MB\cos^2\theta}{2ad\alpha\cos^2\theta+MBac} \end{bmatrix} \begin{bmatrix}e_{11}\\ e_{22}\\ e_{12}\\ e_{21}\end{bmatrix}. \tag{4}$$

Note that the proposed MAMM lattice exhibits asymmetric stress and allows for the presence of a zero mode, denoted as $\mathbf{e}_{zm} = \mathbf{e}_1\otimes\mathbf{e}_2 - \left(a\sin\theta/b\cos\theta\right)\mathbf{e}_2\otimes\mathbf{e}_1$, which meets the requirements of the described transformation method.

3.2 Identification of the design parameters

By comparing Hooke's law of the MAMM (Eq. (4)) and that of the cloak (Eq. (1)), we can obtain the design parameters of the MAMM lattice for a target elastic cloaking,

$$\begin{aligned} MB &= \frac{\lambda\mu}{\lambda-\mu}\frac{a\left(1-g\right)}{cg}, \\ \alpha &= 2\left(\lambda+\mu\right)\sqrt{\frac{\lambda}{2\mu+\lambda}}, \qquad \beta = \frac{2\mu\left(\lambda+\mu\right)}{\lambda}\sqrt{\frac{\lambda}{2\mu+\lambda}}, \\ \theta &= \arctan\sqrt{\frac{\lambda}{2\mu+\lambda}}, \qquad \frac{a}{b} = g\sqrt{\frac{2\mu+\lambda}{\lambda}}. \end{aligned} \tag{5}$$

To illustrate the performance of the MAMM-based cloak, we consider the case $\lambda = \mu$, which enforces

$$MB\to\infty,\ \ \theta = \frac{\pi}{6},\ \ \alpha = \frac{4}{\sqrt{3}}\mu,\ \ \beta = \frac{4}{\sqrt{3}}\mu,\ \ \frac{a}{b} = g\sqrt{3}. \tag{6}$$

In this case, the magneto-mechanical coupling is strong enough and the rotation of the hMAE block

is completely prohibited. Consider that the lattice cloak consists of N angular sectors and P layers (as illustrated in Fig. 2a), the characteristic edge sizes for units located in the k-th layer are $b_{(k)} = 2\pi\left\|\mathbf{x}_{(k)}\right\| / N$ and $a_{(k)} = 2\sqrt{3}\pi\left(\left\|\mathbf{x}_{(k)}\right\| - r_i\right) / N$. Here $\left\|\mathbf{x}_{(k)}\right\|$ denotes the radius position of the k-th layer. Note that the radius of the inner layer of the lattice, i.e., $r_i' = \left\|\mathbf{x}_{(1)}\right\|$, approaches the theoretical cloak inner radius r_i in the limit $P \to +\infty$. The last step in designing the cloak is to determine the microstructure of the springs (with stiffnesses α and β).

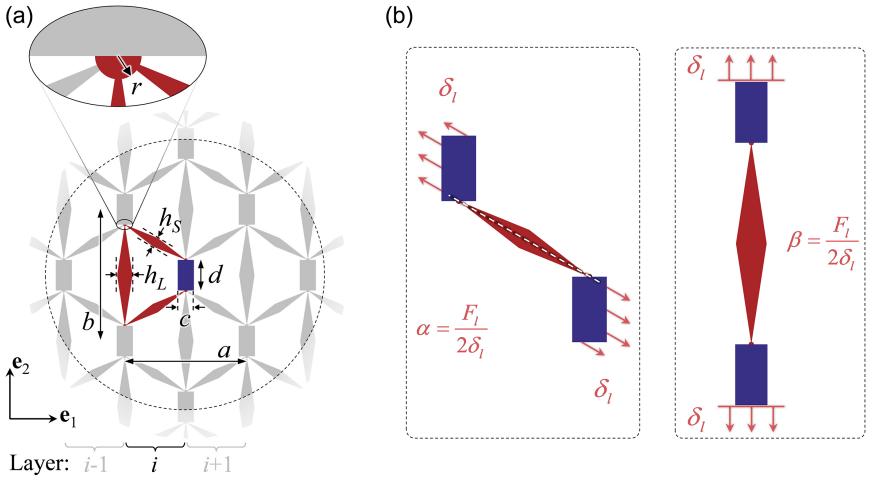

Fig. 3. (a) The microstructure of the MAMM: the rhomboid beams act as springs; the hinge-like contacts are jointed using a semicircle. (b) Finite element simulations for the calculation of the stiffness of the rhomboid beams.

The microstructure of the proposed MAMM – corresponding to the discrete mass-spring model shown in Fig. 2b – is presented in Fig. 3a. Here, the rhomboid beams act as springs, and the hinge-like contacts are jointed using a semicircle with radius r. The stiffnesses of diagonal and vertical rhomboid beams can be determined via finite element simulations of the responses of two mass blocks connected by a single beam. The numerical models, together with the load and boundary conditions, are illustrated in Fig. 3b. To determine the stiffness values of α and β, a displacement δ_l is applied along the direction of the major axis of the rhombus. The stiffness can be calculated by measuring the reaction forces F_l (obtained by the sum of all reaction forces at the nodes located on one of the two boundaries). Combining with optimization method, the characteristic widths (h_S and h_L; see Fig. 3a) of the beams corresponding to the target stiffness (given in Eq. (6)) can be determined. Altogether, the geometric parameters for unit cells located in each layer of the lattice cloak are obtained for given background material parameters (λ and μ), numbers of sectors and layers (N and P), void radius r_i', and the theoretical cloak inner radius r_i.

3.3 Geometry and numerical homogenization of the lattice cloak

To validate the applicability of the proposed MAMM and the corresponding design procedure, a MAMM-based lattice coating with an outer radius of $r_c = 300$ mm, comprising $N = 40$ sectors and $P = 14$ layers, is designed to cloak a void with a radius of $r_i' = 150$ mm. The theoretical inner radius corresponding to the designed lattice cloak is $r_i = 120$ mm. According to the parameter identification procedure in Section 3.2, the geometric parameters of unit cells at different positions in the lattice cloak are given in Table 1. In the numerical simulations throughout this paper, the plane strain hypothesis is adopted. The isotropic background has Lame's constants $\lambda = \mu = 8.2 \times 10^4$ Pa , and the rhomboid beams in the MAMM lattice are characterized by $E = 5$ MPa and $\nu = 0.33$. The hMAE mass blocks in the MAMM lattice are modeled with a sufficiently large modulus (100 times that of the beams), and have remanent magnetization $M = 6.4 \times 10^4$ A / m . The magnetization direction of all hMAE mass blocks in the undeformed state is the same as that of the applied magnetic field B.

Table 1. Geometry parameters of unit cell located in each layer of the lattice cloak.

Layer (k)	$\|\|\mathbf{x}_{(k)}\|\|$ (mm)	$a_{(k)}$ (mm)	$b_{(k)}$ (mm)	$c_{(k)}$ (mm)	$d_{(k)}$ (mm)	$r_{(k)}$ (mm)	$h_{L(k)}$ (mm)	$h_{S(k)}$ (mm)
1	150.00	8.16	23.56	3.00	4.71	0.21	1.87	0.42
2	154.08	9.27	24.20	5.00	4.71	0.23	1.93	0.49
3	158.72	10.53	24.93	5.00	4.71	0.25	2.01	0.57
4	163.98	11.97	25.76	6.00	4.71	0.27	2.10	0.66
5	169.97	13.59	26.70	6.00	4.71	0.29	2.21	0.76
6	176.76	15.44	27.77	8.00	4.71	0.31	2.34	0.89
7	184.49	17.54	28.98	8.00	4.71	0.33	2.50	1.03
8	193.26	19.93	30.36	10.00	4.71	0.35	2.68	1.21
9	203.23	22.64	31.92	10.00	4.71	0.37	2.89	1.41
10	214.55	25.72	33.70	13.00	4.71	0.39	3.14	1.64
11	227.41	29.22	35.72	13.00	4.71	0.41	3.43	1.91
12	242.02	33.20	38.02	15.00	4.71	0.43	3.77	2.23
13	258.62	37.71	40.62	15.00	4.71	0.45	4.16	2.60
14	277.48	42.84	43.59	17.00	4.71	0.47	4.62	3.03

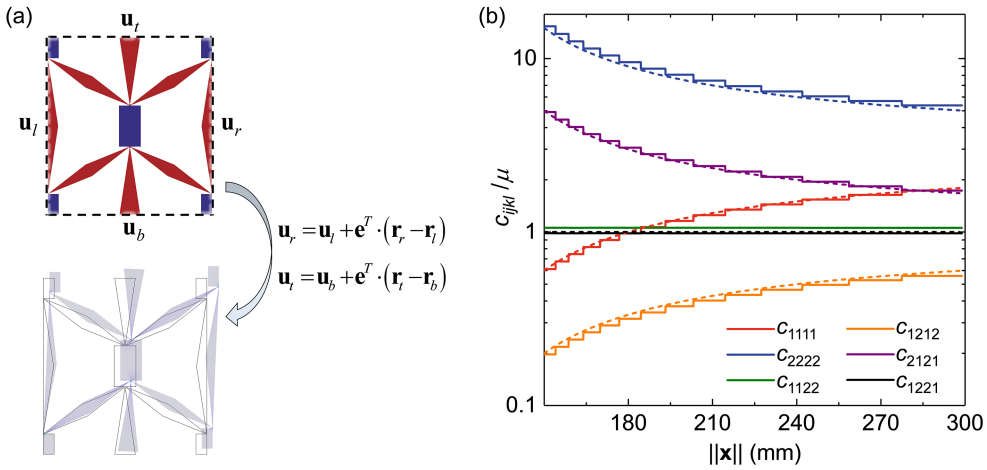

Fig. 4. (a) Boundary condition in the numerical homogenization of the asymmetric metamaterials. (b) The homogenized elasticity tensor for the unit cells at different positions in the MAMM-based cloak. The dotted curves and the solid stepped lines show the theoretical and numerical effective (or homogenized) properties, respectively.

To examine the effective elasticity tensor of the unit cells located at each layer $||\mathbf{x}_{(k)}||$ of the designed lattice cloak, a numerical homogenization procedure is performed. In the numerical simulations, a representative cell is loaded with respect to a given uniform displacement gradient. The applied periodic boundary condition corresponding to the given uniform displacement gradient is illustrated in Fig. 4a. Note that the mass blocks nodes are constrained to experience equal displacements, effectively preventing any rotations. The strain energy density of the homogenized effective media can then be numerically obtained as $\psi = W / ab$, where W is the total strain energy of the representative cell, and ab is its area. Consider six uniform displacement gradients with the following components respectively,

$$\begin{aligned}
[e_{11}\ e_{22}\ e_{12}\ e_{21}] &= [1\ 0\ 0\ 0]e_0, \\
[e_{11}\ e_{22}\ e_{12}\ e_{21}] &= [0\ 1\ 0\ 0]e_0, \\
[e_{11}\ e_{22}\ e_{12}\ e_{21}] &= [1\ 1\ 0\ 0]e_0, \\
[e_{11}\ e_{22}\ e_{12}\ e_{21}] &= [0\ 0\ 1\ 0]e_0, \\
[e_{11}\ e_{22}\ e_{12}\ e_{21}] &= [0\ 0\ 0\ 1]e_0, \\
[e_{11}\ e_{22}\ e_{12}\ e_{21}] &= [0\ 0\ 1\ 1]e_0,
\end{aligned} \tag{7}$$

where $e_0 << 1$ denotes the magnitude of the displacement gradient. The non-zero components of the homogenized elasticity tensor are obtained as,

$$
\begin{aligned}
c_{1111} &= 2\psi_1 / e_0^2, \\
c_{2222} &= 2\psi_2 / e_0^2, \\
c_{1122} &= \left(\psi_3 - \psi_1 - \psi_2\right) / e_0^2, \\
c_{1212} &= 2\psi_4 / e_0^2, \\
c_{2121} &= 2\psi_5 / e_0^2, \\
c_{1221} &= \left(\psi_6 - \psi_4 - \psi_5\right) / e_0^2,
\end{aligned}
\tag{8}
$$

where $\psi_i \left(i = 1,\ 2,\ ...,\ 6\right)$ are the strain energy densities corresponding to the six uniform displacement gradients, respectively. As shown in Fig. 4b, the numerical homogenized effective properties (the solid stepped lines) agree well with the analytical values (the dotted lines) given in Eq. (1).

4 Performance of the MAMM-based cloak

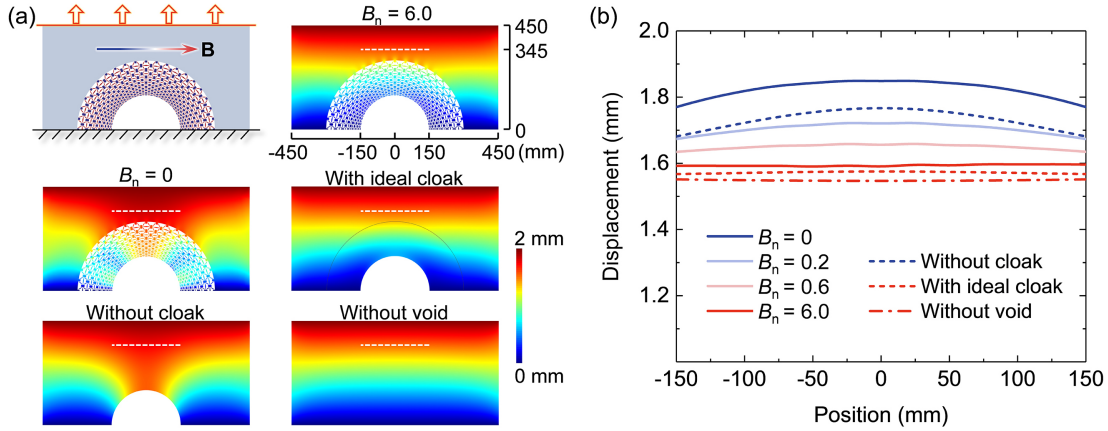

Fig. 5. The performance of the MAMM-based cloak under a uniform tension loading. (a) The total displacement field for cases: void coated by the MAMM-based cloak under different magnetic field levels, void without cloak, void coated by an ideal cloak, and the reference system without void. (b) The total displacement profile measured at the white dashed line (marked in (a), from $-r_i'$ to r_i' in the x-axis, and at $2.3r_i'$ in the y-axis) for these considered cases.

Next, numerical simulations of the performance of the MAMM-based cloak are conducted using the finite element method (COMSOL Multiphysics 6.0). The numerical model consisting of a void coated by the MAMM-based cloak is illustrated in Fig. 5a. Note that we consider the half-cloak model to save computational cost. The bottom of the system is fixed, while a uniform vertical displacement (i.e., a uniform tension loading) is imposed on the top boundary. We record the responses of the system for various levels of external applied magnetic field *B*. For comparison, three other cases are considered: void without cloak, void coated by an ideal cloak, and the reference system without void. Here, the "ideal" cloak is made of a *fictitious* asymmetric medium, with its

material parameters given in Eq. (1). For each case, the total displacement profile at the white dashed line (see in Fig. 5a, from $-r_i'$ to r_i' in the x-axis, and at $2.3r_i'$ in the y-axis) is measured, as shown in Fig. 5b. The normalized magnetic field level is defined as $B_n = MB/\mu$. Clearly, as the external magnetic field level increases, the response of the system with the MAMM cloak approaches that of the system with the ideal cloak. In particular, when the magnetic field level is large enough (such as $B_n = 6.0$), the performance of the proposed MAMM cloak matches well with that of the ideal cloak; both of them effectively make the void indistinguishable from the background medium.

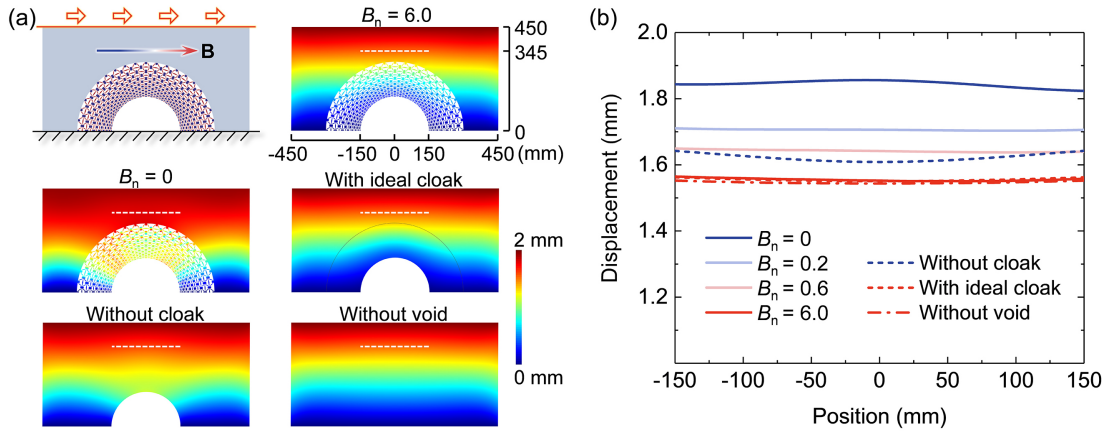

Fig. 6. The performance of the MAMM-based cloak under shear loading. (a) The total displacement field for cases: void coated by the MAMM-based cloak under different magnetic field levels, void without cloak, void coated by an ideal cloak, and the reference system without void. (b) The total displacement profile measured at the white dashed line (marked in (a), from $-r_i'$ to r_i' in the x-axis, and at $2.3r_i'$ in the y-axis) for these considered cases.

Note that due to the isotropy and linearity assumptions, our proposed MAMM-based cloak consistently delivers good cloaking performance for various static loading situations. To demonstrate this, the numerical results corresponding to shear loading are shown in Fig. 6. The numerical model and setting (except the direction of the static loading) are identical to that in Fig. 5. One can see that, under a magnetic field with large enough level (such as $B_n = 6.0$), the performance of the proposed MAMM cloak matches well with that of the ideal cloak; both of them effectively make the void indistinguishable from the background medium. Moreover, a general mechanical loading – a combined load consisting of tension and shear displacements with equal magnitude – is imposed on the top boundary of the considered cloak system. The simulation results are presented in Fig. 7, showing good cloaking performance.

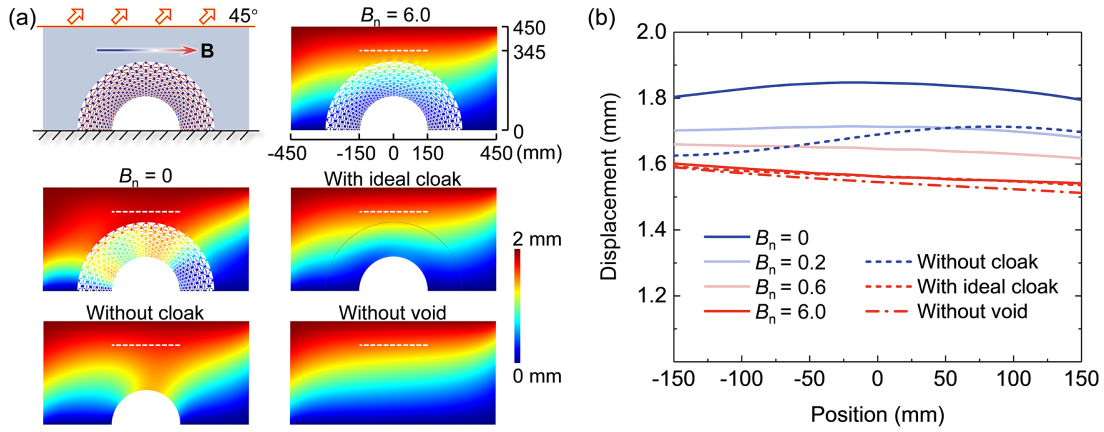

Fig. 7. The performance of the MAMM-based cloak under general mechanical loading. (a) The total displacement field for cases: void coated by the MAMM-based cloak under different magnetic field levels, void without cloak, void coated by an ideal cloak, and the reference system without void. (b) The total displacement profile measured at the white dashed line (marked in (a), from $-r_i'$ to r_i' in the x-axis, and at $2.3r_i'$ in the y-axis) for these considered cases.

Finally, we note that although the proposed MAMM-based cloak is validated in a structural system with a relatively large size scale (a few hundred millimeters, as illustrated Figs. 5-7), our design framework is universal and can be applied to structures with various length scales. In addition, the current study focuses on the case that the background medium has material parameters $\lambda = \mu$ for simplicity. The required magneto-mechanical coupling in this case is very strong (see Eq. (6)) so as to completely prevent the rotation of the hMAE blocks. $B_n = 0.6$ is an example of the magnetic field level that is strong enough for the considered geometric and material parameters (see Figs. 5-7). For background medium with any other material parameters, the required magnetic level can be uniquely determined via Eq. (5).

5 Conclusion

We have proposed a magnetoactive asymmetric mechanical metamaterial for elastic cloaking. The design enables to achieve tunable cloaking without external body torque or rotational resonance effect. The design strategy utilizes the transformative ability of hMAEs coupled with the zero-mode metamaterial characteristics. The interaction between the hMAE intrinsic magnetization and remote magnetic activation gives rise to the unusual asymmetric mechanical behavior (with broken minor symmetry of the effective elasticity tensor of the MAMM). The skewsymmetric component of the stress – representing the micro-moment exerted on the unit cell – is effectively balanced by the magnetic body torque. Such magnetic field-enabled asymmetry can be tuned to achieve the desired material properties required by transformation elasticity and cloaking. A systematic design

procedure is outlined, encompassing the homogenization and inverse design of the microstructural parameters, tailored to specific background media and transformation requirements. We test the responses of the proposed MAMM-based lattice cloak and illustrate the cloaking capability under various static mechanical loadings. Remarkably, thanks to the magneto-mechanical coupling, the MAMM enables us to remotely switch on or off the cloaking performance. Although the results provided here are restricted to statics, they can guide the design of novel tunable cloaking solutions capable of mitigating stress waves and dynamic loads. This study sets a precedent in the field of transformation magneto-elasticity, and opens up opportunities for designing materials to realize transformation media that control elastic deformation or wave and untethered smart devices.

Acknowledgements

QZ thanks the support of the European Unions (EU) Horizon Europe research and innovation funding program through the Marie Skodowska-Curie Actions (Grant No. 101106301- MetaMagic). GH thanks the support of the National Natural Science Foundation of China through Grant No. 11991030. SR thanks for the support of the European Research Council (ERC) through Grant No. 852281- MAGIC.

References

Alam, Z., Padmanabhan, S., Sharma, A.K., 2023. Magnetically tunable longitudinal wave band gaps in hard-magnetic soft laminates. International Journal of Mechanical Sciences 249, 108262.

Bertoldi, K., Vitelli, V., Christensen, J., van Hecke, M., 2017. Flexible mechanical metamaterials. Nature Reviews Materials 2, 17066.

Bilal, O.R., Foehr, A., Daraio, C., 2017a. Bistable metamaterial for switching and cascading elastic vibrations. Proceedings of the National Academy of Sciences of the United States of America 114, 4603-4606.

Bilal, O.R., Foehr, A., Daraio, C., 2017b. Reprogrammable Phononic Metasurfaces. Advanced Materials 29, 1700628.

Brun, M., Guenneau, S., Movchan, A.B., 2009. Achieving control of in-plane elastic waves. Applied Physics Letters 94, 061903.

Buckmann, T., Kadic, M., Schittny, R., Wegener, M., 2015. Mechanical cloak design by direct lattice transformation. Proceedings of the National Academy of Sciences of the United States of America 112, 4930.

Buckmann, T., Thiel, M., Kadic, M., Schittny, R., Wegener, M., 2014. An elasto-mechanical unfeelability cloak made of pentamode metamaterials. Nature Communications 5, 4130.

Chen, T., Pauly, M., Reis, P.M., 2021a. A reprogrammable mechanical metamaterial with stable memory. Nature 589, 386-390.

Chen, Y., Liu, X., Hu, G., 2019. Topological phase transition in mechanical honeycomb lattice. Journal of the Mechanics and Physics of Solids 122, 54-68.

Chen, Y., Zhang, Q., Zhang, Y., Xia, B., Liu, X., Zhou, X., Chen, C., Hu, G., 2021b. Research progress of elastic topological materials. Advances in Mechanics 51, 189-256.

Chen, Y., Zheng, M., Liu, X., Bi, Y., Sun, Z., Xiang, P., Yang, J., Hu, G., 2017. Broadband solid cloak for underwater acoustics. Physical Review B 95, 180104.

Cummer, S.A., Schurig, D., 2007. One path to acoustic cloaking. New Journal of Physics 9, 45.

Ergin, T., Stenger, N., Brenner, P., Pendry, J.B., Wegener, M., 2010. Three-Dimensional Invisibility Cloak at Optical Wavelengths. Science 328, 337.

Goshkoderia, A., Chen, V., Li, J., Juhl, A., Buskohl, P., Rudykh, S., 2020. Instability-induced pattern formations in soft magnetoactive composites. Physical Review Letters 124, 158002.

Greenleaf, A., Lassas, M., Uhlmann, G., 2003. Anisotropic conductivities that cannot be detected by EIT. Physiological Measurement 24, 413.

Gross, M.F., Schneider, J.L.G., Wei, Y., Chen, Y., Kalt, S., Kadic, M., Liu, X., Hu, G., Wegener, M., 2023. Tetramode Metamaterials as Phonon Polarizers. Advanced Materials 35, e2211801.

Guo, D., Zhang, Q., Hu, G., 2022. Rational design of hyperelastic semi-linear material and its application to elastic wave control. Mechanics of Materials 166, 104237.

Hu, W., Lum, G.Z., Mastrangeli, M., Sitti, M., 2018. Small-scale soft-bodied robot with multimodal locomotion. Nature 554, 81-85.

Kheybari, M., Bilal, O.R., 2023. Harnessing asymmetry to reprogram nonlinear metamaterials on-the-fly with no moving parts. Materials & Design 233, 112168.

Kim, Y., Yuk, H., Zhao, R., Chester, S.A., Zhao, X., 2018. Printing ferromagnetic domains for untethered fast-transforming soft materials. Nature 558, 274-279.

Krushynska, A.O., Torrent, D., Aragón, A.M., Ardito, R., Bilal, O.R., Bonello, B., Bosia, F., Chen, Y., Christensen, J., Colombi, A., Cummer, S.A., Djafari-Rouhani, B., Fraternali, F., Galich, P.I., Garcia, P.D., Groby, J.-P., Guenneau, S., Haberman, M.R., Hussein, M.I., Janbaz, S., Jiménez, N., Khelif, A., Laude, V., Mirzaali, M.J., Packo, P., Palermo, A., Pennec, Y., Picó, R., López, M.R., Rudykh, S., Serra-Garcia, M., Sotomayor Torres, C.M., Starkey, T.A., Tournat, V., Wright, O.B., 2023. Emerging topics in nanophononics and elastic, acoustic, and mechanical metamaterials: an overview. Nanophotonics 12, 659-686.

Lee, K.H., Al Babaa, H., Yu, K., Li, K., Zhang, Y., Du, H., Masri, S.F., Wang, Q., 2022. Magnetoactive Acoustic Topological Transistors. Advanced Science 9, e2201204.

Leonhardt, U., 2006. Optical Conformal Mapping. Science 312, 1777.

Liu, H., Zhang, Q., Zhang, K., Hu, G., Duan, H., 2019. Designing 3D Digital Metamaterial for Elastic Waves: From Elastic Wave Polarizer to Vibration Control. Advanced Science 6, 1900401.

Lucarini, S., Hossain, M., Garcia-Gonzalez, D., 2022. Recent advances in hard-magnetic soft composites: Synthesis, characterisation, computational modelling, and applications. Composite Structures 279, 114800.

Lum, G.Z., Ye, Z., Dong, X., Marvi, H., Erin, O., Hu, W., Sitti, M., 2016. Shape-programmable magnetic soft matter. Proceedings of the National Academy of Sciences of the United States of America 113, E6007-E6015.

Memoli, G., Caleap, M., Asakawa, M., Sahoo, D.R., Drinkwater, B.W., Subramanian, S., 2017. Metamaterial bricks and quantization of meta-surfaces. Nature Communications 8, 14608.

Milton, G.W., Briane, M., Willis, J.R., 2006. On cloaking for elasticity and physical equations with a transformation invariant form. New Journal of Physics 8, 248-248.

Montgomery, S.M., Wu, S., Kuang, X., Armstrong, C.D., Zemelka, C., Ze, Q., Zhang, R., Zhao, R., Qi, H.J., 2020. Magneto‐mechanical metamaterials with widely tunable mechanical properties and acoustic bandgaps. Advanced Functional Materials 31, 2005319.

Moreno-Mateos, M.A., Hossain, M., Steinmann, P., Garcia-Gonzalez, D., 2022. Hybrid magnetorheological elastomers enable versatile soft actuators. npj Computational Materials 8, 162.

Mukherjee, D., Rambausek, M., Danas, K., 2021. An explicit dissipative model for isotropic hard magnetorheological elastomers. Journal of the Mechanics and Physics of Solids 151, 104361.

Nassar, H., Chen, Y.Y., Huang, G.L., 2018. A degenerate polar lattice for cloaking in full two-dimensional elastodynamics and statics. Proceedings of the Royal Society A: Mathematical, Physical and Engineering Sciences 474, 20180523.

Nassar, H., Chen, Y.Y., Huang, G.L., 2019. Isotropic polar solids for conformal transformation elasticity and cloaking. Journal of the Mechanics and Physics of Solids 129, 229-243.

Nassar, H., Chen, Y.Y., Huang, G.L., 2020. Polar metamaterials: A new outlook on resonance for cloaking applications. Physical Review Letters 124, 084301.

Norris, A.N., 2008. Acoustic cloaking theory. Proceedings of the Royal Society A: Mathematical, Physical and Engineering Sciences 464, 2411-2434.

Norris, A.N., Parnell, W.J., 2012. Hyperelastic cloaking theory: transformation elasticity with pre-stressed solids. Proceedings of the Royal Society A: Mathematical, Physical and Engineering Sciences 468, 2881-2903.

Pan, F., Li, Y., Li, Z., Yang, J., Liu, B., Chen, Y., 2019. 3D Pixel Mechanical Metamaterials. Advanced Materials 31, e1900548.

Parnell, W.J., 2012. Nonlinear pre-stress for cloaking from antiplane elastic waves. Proceedings of the Royal Society A: Mathematical, Physical and Engineering Sciences 468, 563-580.

Pendry, J.B., Schurig, D., Smith, D.R., 2006. Controlling Electromagnetic Fields. Science 312, 1780.

Sim, J., Wu, S., Dai, J., Zhao, R.R., 2023. Magneto-Mechanical Bilayer Metamaterial with Global Area-Preserving Density Tunability for Acoustic Wave Regulation. Advanced Materials 35, e2303541.

Sim, J., Zhao, R.R., 2023. Magneto-Mechanical Metamaterials: A Perspective. Journal of Applied Mechanics 91, 031004.

Wang, L., Chen, Z., Cheng, L., 2023. A metamaterial plate with magnetorheological elastomers and gradient resonators for tuneable, low-frequency and broadband flexural wave manipulation. Thin-Walled Structures 184, 110521.

Wang, L., Zheng, D., Harker, P., Patel, A.B., Guo, C.F., Zhao, X., 2021. Evolutionary design of magnetic soft continuum robots. Proceedings of the National Academy of Sciences of the United States of America 118, e2021922118.

Wang, P., Lu, L., Bertoldi, K., 2015. Topological Phononic Crystals with One-Way Elastic Edge Waves. Physical Review Letters 115, 104302.

Wang, Y.-F., Wang, Y.-Z., Wu, B., Chen, W., Wang, Y.-S., 2020. Tunable and active phononic crystals and metamaterials. Applied Mechanics Reviews 72, 040801.

Wang, Y., Ramirez, B., Carpenter, K., Naify, C., Hofmann, D.C., Daraio, C., 2019. Architected lattices with adaptive energy absorption. Extreme Mechanics Letters 33, 100557.

Wang, Z., Zhang, Q., Zhang, K., Hu, G., 2016. Tunable Digital Metamaterial for Broadband Vibration Isolation at Low Frequency. Advanced Materials 28, 9857-9861.

Watkins, A.A., Eichelberg, A., Bilal, O.R., 2022. Harnessing Reprogrammable Phase Transitions to Control the Propagation of Sound Waves. Physical Review Applied 17, 024036.

Wei, Y., Liu, X., Hu, G., 2021. Quadramode materials: Their design method and wave property.

Materials & Design 210, 110031.

Xu, X., Wang, C., Shou, W., Du, Z., Chen, Y., Li, B., Matusik, W., Hussein, N., Huang, G., 2020. Physical Realization of Elastic Cloaking with a Polar Material. Physical Review Letters 124, 114301.

Yan, D., Abbasi, A., Reis, P.M., 2021a. A comprehensive framework for hard-magnetic beams: Reduced-order theory, 3D simulations, and experiments. International Journal of Solids and Structures 257, 111319.

Yan, D., Aymon, B.F.G., Reis, P.M., 2023. A reduced-order, rotation-based model for thin hard-magnetic plates. Journal of the Mechanics and Physics of Solids 170, 105095.

Yan, D., Pezzulla, M., Cruveiller, L., Abbasi, A., Reis, P.M., 2021b. Magneto-active elastic shells with tunable buckling strength. Nature Communications 12, 2831.

Yang, X., Keten, S., 2023. Emergent elasticity relations for networks of bars with sticky magnetic ends. Extreme Mechanics Letters 65, 102093.

Zhang, H.K., Chen, Y., Liu, X.N., Hu, G.K., 2020a. An asymmetric elastic metamaterial model for elastic wave cloaking. Journal of the Mechanics and Physics of Solids 135, 103796.

Zhang, Q., Chen, Y., Zhang, K., Hu, G., 2020b. Dirac degeneracy and elastic topological valley modes induced by local resonant states. Physical Review B 101, 014101.

Zhang, Q., Cherkasov, A.V., Arora, N., Hu, G., Rudykh, S., 2023a. Magnetic field-induced asymmetric mechanical metamaterials. Extreme Mechanics Letters 59, 101957.

Zhang, Q., Cherkasov, A.V., Xie, C., Arora, N., Rudykh, S., 2023b. Nonlinear elastic vector solitons in hard-magnetic soft mechanical metamaterials. International Journal of Solids and Structures 280, 112396.

Zhang, Q., Guo, D., Hu, G., 2021. Tailored Mechanical Metamaterials with Programmable Quasi-Zero-Stiffness Features for Full-Band Vibration Isolation. Advanced Functional Materials 31, 2101428.

Zhang, Q., Rudykh, S., 2022. Magneto-deformation and transverse elastic waves in hard-magnetic soft laminates. Mechanics of Materials 169, 104325.

Zhang, W., Zhou, J., Jia, Y., Chen, J., Pu, Y., Fan, R., Meng, F., Ge, Q., Lu, Y., 2023c. Magnetoactive microlattice metamaterials with highly tunable stiffness and fast response rate. NPG Asia Materials 15, 45.

Zhang, X., Xiao, M., Cheng, Y., Lu, M.-H., Christensen, J., 2018. Topological sound. Communications Physics 1, 97.

Zhao, R., Kim, Y., Chester, S.A., Sharma, P., Zhao, X., 2019. Mechanics of hard-magnetic soft materials. Journal of the Mechanics and Physics of Solids 124, 244-263.

Zhu, R., Liu, X.N., Hu, G.K., Sun, C.T., Huang, G.L., 2014. Negative refraction of elastic waves at the deep-subwavelength scale in a single-phase metamaterial. Nature Communications 5, 5510.